Semidiurnal Tides on the Laptev Sea Shelf with Implications for Shear and Vertical Mixing

MARKUS A. JANOUT

Alfred Wegener Institute, Helmholtz Centre for Polar and Marine Research, Bremerhaven, Germany

YUENG-DJERN LENN

School of Ocean Sciences, Bangor University, Anglesey, United Kingdom

(Manuscript received 12 December 2012, in final form 10 October 2013)

ABSTRACT

The Arctic continental shelf seas hold a globally significant source of freshwater that impacts Arctic Ocean stratification, circulation, and climate. This freshwater can be injected below the surface mixed layer by intense turbulent kinetic energy dissipation events, as resolved by Laptev Sea microstructure observations. The tides provide a major source of energy that can be dissipated and hence drive diapycnal mixing in the Laptev Sea. Multiyear ADCP mooring records from locations across the shelf reveal that semidiurnal tides are dominated by the M_2 and S_2 constituents, with the largest amplitudes on the outer shelf. Throughout most of the shelf, tides are clockwise polarized and sheared by stratification, as characteristic near the M_2 critical latitude. Interannual variations of the tidal and shear structures on the inner shelf are mainly determined by the stratification-setting Lena River freshwater plume. In all locations, M_2 tides are enhanced under sea ice, and therefore changes in the seasonal ice cover may lead to changes in tides and water column structure. The main conclusions of this study are that (i) tides play a comparatively greater role year-round on the outer shelf relative to the inner shelf; (ii) a sea ice reduction will overall decrease the predictability of the currents, especially on the inner shelf; and (iii) the freshwater distribution directly impacts diapycnal mixing by setting the vertical tidal structure. These combined effects imply that future sea ice loss will increase the variability and vertical mixing of freshwater, particularly on the inner shelf, where the Lena River first enters the Laptev Sea.

1. Introduction

The Siberian shelves are vast and shallow and comprise a large part of the total Arctic shelf area (Fig. 1). More than 80% of the Arctic freshwater input originates from Eurasian landmasses (Peterson et al. 2002; Holland et al. 2006) and enters the Siberian shelves—in particular, from the Ob, Yenisei, and Lena—three of the largest rivers on Earth, which shape the hydrographic and biogeochemical environment in these regions. Nevertheless, the Siberian shelves are among the least studied shelf seas on the planet and host a complex series of processes impacted by freshwater, Atlantic-derived basin water, sea ice, polynyas, and tides. As a representative of the Siberian shelves, the Laptev Sea, located between the Kara and East Siberian Seas, is an important ice formation and export region (Alexandrov et al. 2000; Krumpen et al. 2013) and the beginning of the Transpolar Drift system. Nearly half of the Laptev Sea is covered by landfast ice in winter, and polynyas frequently open along the landfast ice edge (Zakharov 1966; Bareiss and Görgen 2005). The Lena River freshwater controls stratification and carries suspended material (Wegner et al. 2013) and colored dissolved organic matter (Stedmon et al. 2011), regulating the light availability and the biological productivity on this shelf. Exchange mechanisms between coastal freshwater and Atlantic-derived water masses across the steep continental slope are crucial although not sufficiently understood. Undoubtedly, understanding the Laptev Sea ecosystem requires a comprehensive understanding of the mechanisms governing the freshwater distribution and variability.

The horizontal distribution of the Lena River freshwater is first-order dependent on the large-scale summer winds (Shpaikher et al. 1972), and hence it shows

Corresponding author address: Markus Janout, Alfred Wegener Institute, Helmholtz Centre for Polar and Marine Research, Am Handelshafen 12, D-27570 Bremerhaven, Germany.
E-mail: markus.janout@awi.de

DOI: 10.1175/JPO-D-12-0240.1

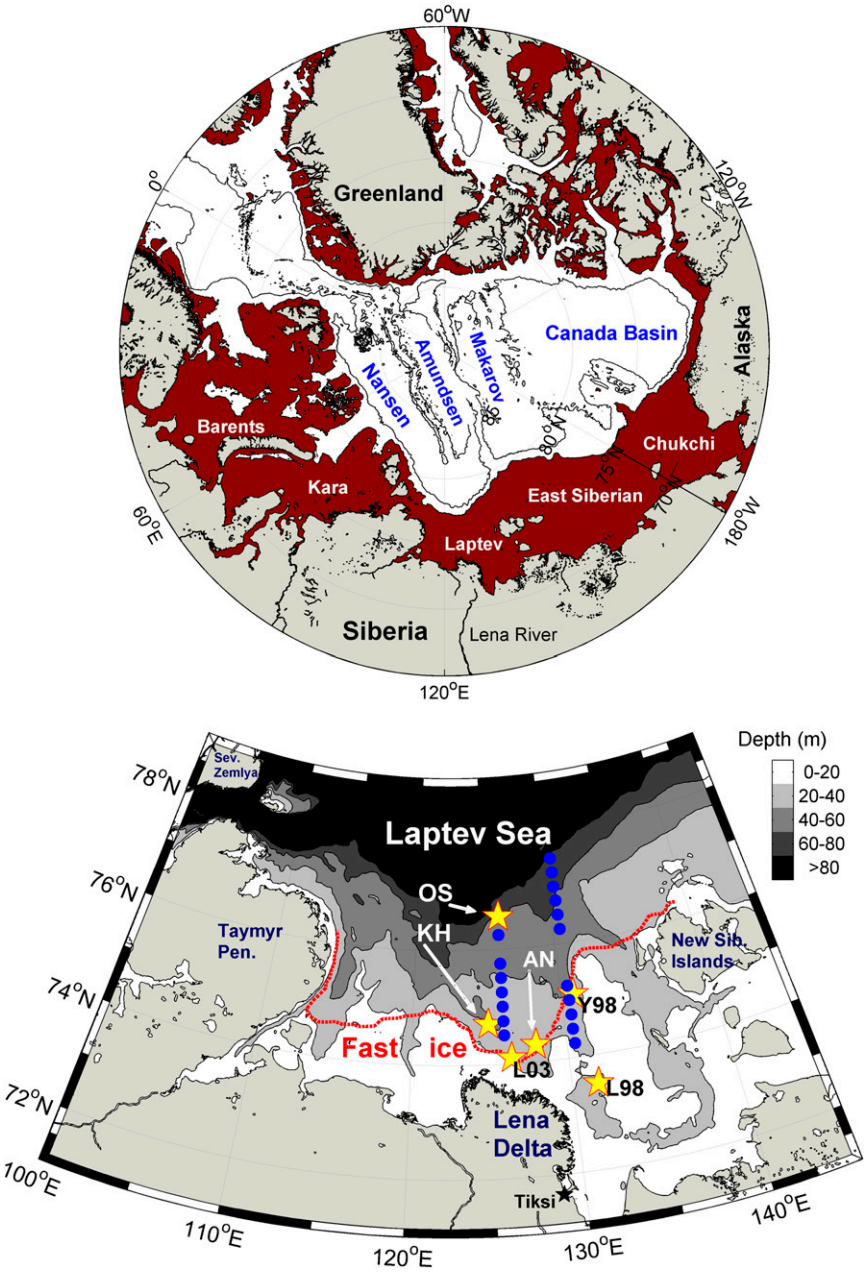

FIG. 1. (top) Map of the Arctic Ocean including the 300- and 2000-m isobaths (black contours) based on the IBCAO (Jakobsson et al. 2008). Red shading marks shelf regions from 0 to 300 m; the Laptev Sea region of interest is found at the bottom of the map. (bottom) Map of the Laptev Sea. Yellow stars indicate year-round mooring locations including their denotations as used in the text. Blue dots show VMP stations. Note that there are gaps in the transects. The landfast ice edge is outlined with the March 2010 fast ice edge [red dashed line, from Janout et al. (2013)]. The bathymetry is also based on IBCAO.

considerable interannual variability (Guay et al. 2001; Dmitrenko et al. 2010). During summers with predominantly offshore-directed winds, freshwater is advected offshore and to the East Siberian Sea, leading to anomalously weak stratification in the central Laptev Sea. Onshore-directed winds, on the other hand, accumulate freshwater on the shelf and cause strong stratification, which may persist through the following winter (Bauch et al. 2009; Dmitrenko et al. 2010). However, those processes controlling diapycnal mixing to vertically

redistribute energy and matter remain poorly understood. Unlike the rather quiescent Arctic Basin (Rainville and Winsor 2008; Fer 2009), where double diffusion is a dominant mixing process (Rudels et al. 1999; Timmermans et al. 2008; Polyakov et al. 2012), Arctic shelves are known to include regions that are characterized by enhanced dissipation rates of turbulent kinetic energy ε. These are mainly related to tides and/or flow over variable topography (Padman and Dillon 1991; D'Asaro and Morison 1992; Sundfjord et al. 2007; Fer et al. 2010).

The critical latitude, where a tidal frequency equals the inertial frequency f, is known to affect certain tidal characteristics such as baroclinicity and potentially large boundary layers (Foldvik et al. 1990; Nøst 1994; Robertson 2001; Makinson et al. 2006). Kulikov et al. (2004) describe strongly baroclinic semidiurnal tides related to resonant generation of internal tides near the N_2 critical latitude (70.98°N) on the Mackenzie shelf break in the Canadian Beaufort Sea. Tidal assimilation models such as the 5-km Arctic Ocean Tidal Inverse Model (AOTIM-5; Padman and Erofeeva 2004) show considerable tidal activity in parts of the Laptev Sea shelf, which is intersected by the M_2 critical latitude (74.47°N). Critical latitude effects may be expected over a wider latitude band given the small meridional gradient of f in this region [$\sim 7 \times 10^{-7}\,\mathrm{s}^{-1}\,(^\circ\mathrm{lat})^{-1}$] and the critical latitude's dependence on the relative vorticity of the background circulation (D'Asaro and Morison 1992; Vlasenko et al. 2003), which is largely unknown in the Laptev Sea. Hence, the setup on the Laptev Sea shelf involves tides near the critical latitude combined with strong stratification and may lead to conditions favorable for enhanced tide-induced diapycnal mixing. Nevertheless, observations there are scarce and only a limited number of scientific contributions are specialized on the effect of tides on mixing. For instance, Dmitrenko et al. (2012) discussed the potential effect of tidal mixing based on current measurements in a coastal polynya, and Lenn et al. (2011, hereafter L11) combined microstructure and current measurements to show intermittent tide-induced mixing events at a northeastern Laptev Sea slope location under 100% ice cover. L11 attributed their observations to a mechanism proposed by Burchard and Rippeth (2009, hereafter BR09), which links intermittent shear spikes to the alignment of the semidiurnally rotating shear vector with the surface forcing.

The goal of this paper is to identify the dominant components of the tides and their relationship with stratification and seasonal ice cover as observed by oceanographic moorings across the Laptev Sea shelf. We further investigate the potential of tides for driving episodes of high ε based on microstructure measurements, and discuss the implications of a changing seasonal ice cover on tides and the mixing environment of the Laptev Sea. The paper is organized as follows. The next section provides background on the mixing environment of the Laptev Sea, followed by a data and methods description in section 3. Section 4 provides the results, including a presentation of the basic tidal characteristics (vertical structure, seasonal, spatial, and interannual variability) and their relationship with shear and sea ice. Discussion and conclusions are given in section 5.

2. Background: Intermittent mixing in the Laptev Sea

Critical latitude effects can result in mixing within very thick tidal top and bottom boundary layers (Foldvik et al. 1990) that can merge into a single mixed layer. In the Laptev Sea, the Lena River plume controls stratification, which can be strong enough to persist throughout the year. This suggests that the tidally driven boundary layers may remain distinct with the mixing inhibited by the persistent stratification. In fact, two cross-shelf microstructure transects (Fig. 1) along 126°E (74.50°–76.25°N, 7 stations) and 130°E (77.50°–74.25°N, 11 stations), respectively, revealed an energetic environment characterized by intermittent high ε events (Fig. 2) during an ice-free late September 2007 (Stroeve et al. 2008). The high ε events occur within a bottom boundary and at the base of the surface mixed layer, raising the obvious question about the mechanisms driving these events.

These microstructure data were collected with a Rockland Scientific International vertical microstructure profiler (VMP)-500 as part of the 2007 Arctic Synoptic Basin-wide Observations (ASBO) program during a joint cruise with the Nansen and Amundsen Basins Observational System (NABOS) research program aboard the Russian Research Vessel *Viktor Buynitsky*. Microstructure shear, temperature, and conductivity profiles from the VMP, in free-fall mode with typical fall speeds of $0.65\,\mathrm{m\,s}^{-1}$, were obtained at each station with approximately four repeat profiles, and were then edited and processed following standard procedures as described by Lenn et al. (2009) to produce estimates of ε. As these microstructure observations were taken along near-synoptic hydrographic sections spanning several hundreds of kilometers, they may not be regarded as a single-location time series usually undertaken in shelf process studies. Consequently, deciphering the role of tides in driving the observed ε requires particularly good knowledge of the phase and vertical character of the tidal currents, as they vary across the shelf.

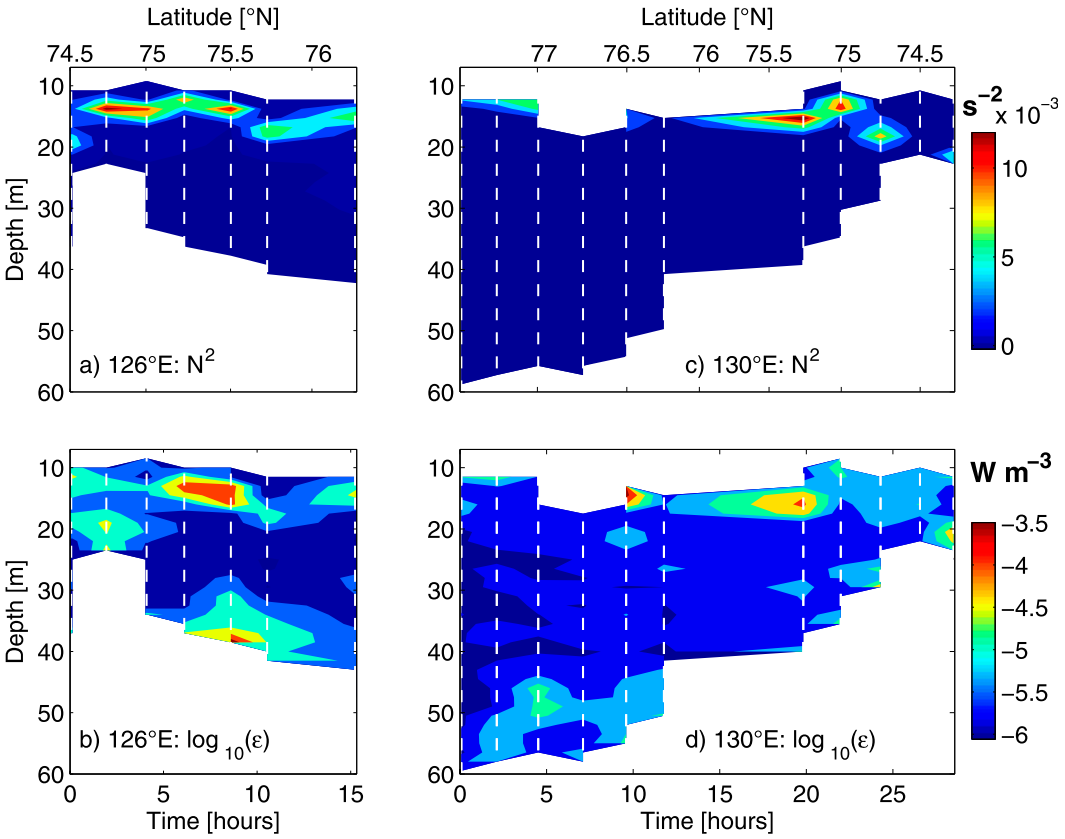

FIG. 2. (a),(b) Western (126°E) and (c),(d) eastern (130°E) VMP transects from September 2007. Buoyancy frequency N^2 (s^{-2}) is given in (a),(c) and ε($W\,m^{-3}$) is given in (b),(d). White vertical dashed lines indicate station locations. Note that there are station gaps in the transects. The x axes for (a),(c) show the occupation hours and the x axes for (b),(d) show the lat for spatial reference (Fig. 1). Note that the 130°E transect was occupied from north to south and the 126°E transect from south to north.

3. Data and methods

a. Moorings

We used data records from six different year-round mooring locations (Fig. 1), each providing between 1 and 4 years of data. The moorings were all operated as part of the German–Russian "Laptev Sea System" project, which is a continuing partnership between German and Russian research institutes begun in 1992. Short abbreviations for mooring identification were chosen from the original mooring names, which with exception of the outer shelf mooring (OS), were based on rivers close to the mooring location: Khatanga (KH), Anabar (AN), Lena (L), and Yana (Y). Besides some minor variations in the instrumentation (Table 1), each mooring was designed to remain a safe distance below the sea ice, and was equipped with Teledyne RD Instruments' upward-looking 300-kHz Workhorse Sentinel acoustic Doppler current profilers (ADCP), profiling the water column in 1–2-m bins with a sampling frequency of 30 min. KH and AN feature an additional downward-looking 1200-kHz ADCP. Each mooring recorded temperature, salinity, and pressure with a near-bottom Sea-Bird Electronics (SBE)-37 conductivity–temperature–depth (CTD) recorder, which was occasionally complemented by unpumped Richard Brancker Research (RBR) Ltd. CTDs, mounted on the ADCP frames. Some deployments made use of the ADCP's bottom-tracking mode, which provided local sea ice information (ice drift and relative ice thickness) above the mooring. The data collection spans three moorings with 2–4-yr-long deployments: OS, KH, and AN. Three single-year records are Y98, L98, and L03, where the numbers indicate the year of deployment. Mooring locations are presented in Fig. 1, and basic information on instruments and recording periods are summarized in Table 1. For a detailed description of the data processing and accuracies of ADCP and CTD data, please refer to Hölemann et al. (2011) or Janout et al. (2013).

b. CTD

The CTD profiles used in this paper were collected during summer (from mid-August to mid-September)

TABLE 1. List of moorings including recording times (RT), instruments, depth, position. CR = complete record, i.e., a yearlong data record from deployment to recovery in late summer. Dates indicate the length of incomplete records. The 300-kHz ADCP are oriented upward (up), and 1200-kHz ADCP are oriented downward (down). RBR conductivity data may be faulty because of sensor drift; quality of temperature data is good.

Mooring	Lat (N)	Lon (E)	Depth (m)	RT	ADCP 300 (up)	ADCP 1200 (down)	Bottom track	SBE37 (bottom)	SBE37 (2)	RBR (1)	RBR (2)
OS	76.73°	125.92°	63	2005/06	25 Apr 2006	N/A	N/A	CR	N/A	N/A	N/A
OS	76.74°	125.92°	64	2006/07	CR	N/A	Yes	CR			
OS	76.57°	126.06°	53	2010/11	CR	N/A	Yes	CR	40 m: CR	N/A	N/A
KH	74.72°	125.29°	43	2007/08	CR	CR	Yes	26 Apr 2008	N/A	CR	CR
KH	74.71°	125.29°	43	2008/09	17 Apr 2009	3 Apr 2009	Yes	CR	N/A	CR	CR
KH	74.72°	125.28°	45	2009/10	CR	CR	Yes	CR	N/A	CR	CR
KH	74.71°	125.25°	42	2010/11	N/A	CR	N/A	CR	19 m: CR	N/A	N/A
AN	74.33°	128.00°	32	2007/08	CR	CR	Yes	N/A	N/A	CR	CR
AN	74.33°	128.01°	33	2008/09	N/A	15 Feb 2009	Yes	5 Jun 2009	N/A	CR	CR
AN	74.33°	128.00°	33	2009/10	CR	CR	Yes	CR	N/A	CR	CR
Y98	75.15°	130.84°	45	1998/99	CR	N/A	N/A	CR	N/A	N/A	N/A
L98	73.46°	131.70°	24	1998/99	CR	N/A	N/A	N/A	N/A	N/A	N/A
L03	74.12°	126.42°	25	2003/04	CR	N/A	Yes	N/A	N/A	N/A	N/A

expeditions to the Laptev Sea from 2007 to 2011, with the exception of one profile, taken in the vicinity of Y98 during a winter expedition during May 1999. The data were collected with SBE SeaCAT profilers (SBE19), which provide initial accuracies for temperature and conductivity of 0.005°C and 0.0005 S m^{-1}, respectively.

c. AOTIM-5

Barotropic tides for the Laptev Sea were derived from AOTIM-5 output (Padman and Erofeeva 2004). This pan-Arctic assimilation model is highly resolved (5-km grid), assimilating data from coastal and benthic tide gauges (between 250 and 310 gauges per tidal constituent) and available satellite altimeters [364 cycles of Ocean Topography Experiment (TOPEX)/Poseidon and 108 cycles of European Remote Sensing Satellite (ERS) altimeter data] to simulate the most energetic tides M_2, S_2, O_1, and K_1, and in addition provides information on N_2, K_2, P_1, and Q_1. Model bathymetry is based on the International Bathymetric Chart of the Arctic Ocean (IBCAO; Jakobsson et al. 2008), and sea ice is not included in the model.

d. Sea ice

Satellite-based sea ice concentration is generated from brightness temperature data derived from the *Nimbus-7* Scanning Multichannel Microwave Radiometer (SMMR), the Defense Meteorological Satellite Program (DMSP) *F8*, *F11*, and *F13* Special Sensor Microwave Imager (SSM/I), and the *F17* Special Sensor Microwave Imager/Sounder (SSM/IS). The approximately daily data are provided by the National Snow and Ice Data Center on a polar stereographic grid with a cell size of 25 km × 25 km (Cavalieri et al. 2008). The ADCP's bottom-tracking function alternatively provides localized information on the presence and absence of sea ice directly above the mooring. When ice is present, the transducer obtains good return signals, while in open water, scattering occurs at the surface and error velocities are high, indicating the absence of sea ice as a solid reflector.

4. Results

a. Dominant modes of variability in currents and shear

ADCP-measured current records from year-round moorings from the Laptev Sea shelf (Fig. 1) were analyzed to determine the role of tides and near-inertial motion on shear and vertical mixing. Initially, the currents were depth averaged and decomposed into rotary components—that is, anticyclonic [clockwise (CW)] and cyclonic [counterclockwise (CCW)]—and then used for a spectral power analysis (Figs. 3a,b; Gonella 1972).

The currents' power spectra are strongly dominated by semidiurnal frequencies at both OS and KH (Fig. 3).

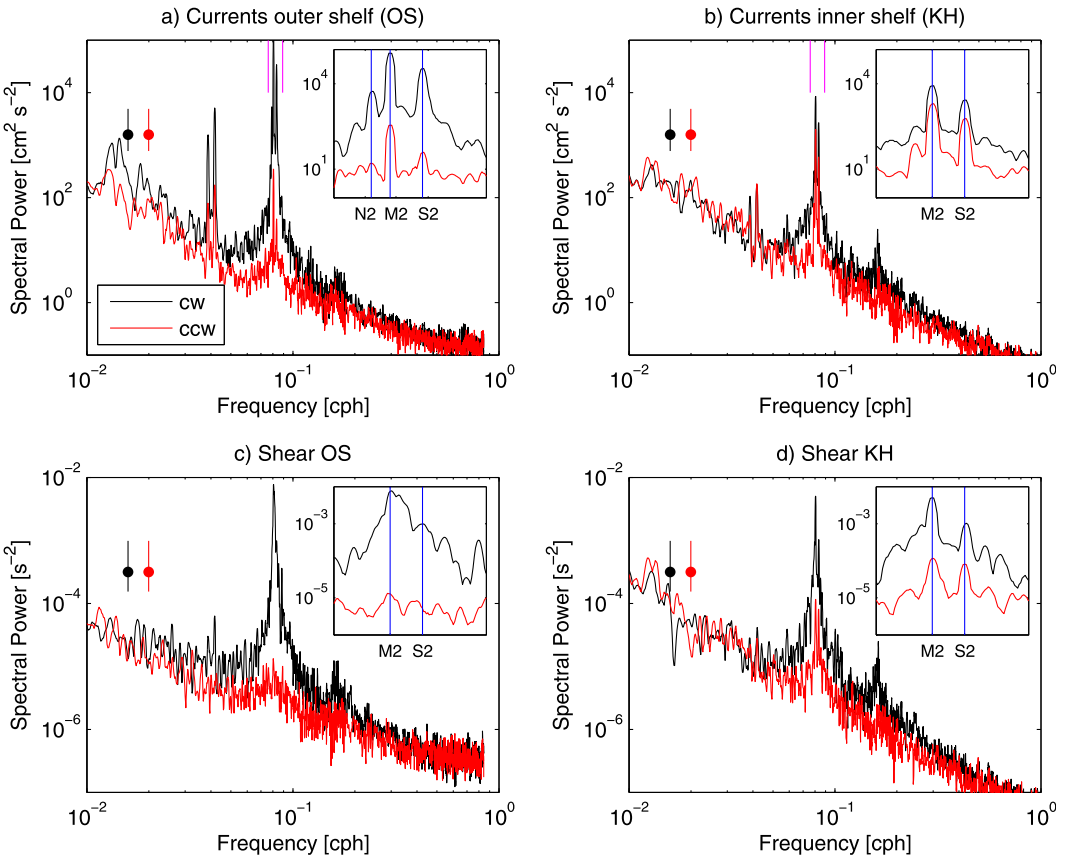

FIG. 3. Spectral power of (a),(b) currents (cm^2 s^{-2}) and (c),(d) shear (s^{-2}) on KH (b),(d) and OS (a),(c) vs frequency [cycles per hour (cph)] on a log–log scale. Semidiurnal frequencies indicated by the magenta lines in (a) and (b) are enlarged in the insert windows. M_2: 0.0805, S_2: 0.0833, and N_2: 0.0789 cph.

The spectra show statistically significant peaks at the M_2 and S_2 frequencies at both sites, and additionally a smaller N_2 peak at OS. At OS, the CW component dominates the CCW component by one order of magnitude. In contrast, at KH the maximum CW component at semidiurnal frequency exceeds that of the CCW component by only a factor of ~4, implying comparatively weaker polarization on the inner shelf. Additional CW-polarized peaks at OS occur at diurnal frequencies (O_1 and K_1), again with weaker but statistically significant peaks in the CCW component. Diurnal frequencies play a minor role on the inner shelf compared to the relatively greater influence at OS and the Laptev Sea slope (Kowalik and Proshutinsky 1993; Padman and Erofeeva 2004).

Shear instabilities that drive diapycnal mixing may arise from baroclinicity in tidal currents. For first-order insights into the role of shear-driven mixing, we computed bulk shear by subtracting averaged lower-layer velocities (40–50 m at OS and 30–40 m at KH) from averaged upper-layer velocities (10–20 m) to capture the cross-pycnocline shear. The layers were chosen based on the depth of the pycnocline indicated by late-summer CTD profiles and the vertical structure of tides presented below. The difference in layer-averaged currents was then divided by the distance between these layers (30 m at OS and 20 m at KH) and decomposed accordingly into rotary spectra (Figs. 3c,d). At OS, the shear spectrum is again dominated by a CW-polarized peak in the semidiurnal band (Fig. 3c). The M_2 and S_2 CCW components as well as the diurnal currents are entirely depth uniform and therefore show no peaks in the shear spectrum. The semidiurnal spectral peak is slightly lower at KH than at OS, and features a comparatively stronger CCW peak (Fig. 3d).

b. Barotropic semidiurnal tides on the Laptev Sea shelf

The relative contribution of the major tidal constituents on the inner and outer shelves as well as their seasonal, interannual, and vertical variability was quantified by carrying out harmonic analysis on the ADCP records using the matrix laboratory (MATLAB) T-Tide package (Pawlowicz et al. 2002). Tidal currents are presented in

TABLE 2. Comparison of ellipse characteristics [major and minor axes (cm s^{-1})] and phase and inclination (°) for the four major semidiurnal tides between ADCP including the 95% confidence and AOTIM-5 at moorings OS, KH, AN, and Y98. The AOTIM5 numbers are boldfaced to make them easier distinguished. Note that the ADCP-derived tides were computed from the year-round records.

	M_2	S_2	N_2	K_2
OS (76.6°N, 126°E)				
Major axis (ADCP)	12.5 ± 0.1	6.5 ± 0.1	2.7 ± 0.09	1.9 ± 0.06
Major axis (AOTIM-5)	**8.9**	**3.7**	**2.9**	**1.1**
Minor axis (ADCP)	−11.5 ± 0.1	−6.2 ± 0.1	−2.5 ± 0.1	−1.7 ± 0.1
Minor axis (AOTIM-5)	**−7.3**	**−3.1**	**−2.3**	**−0.9**
Phase (ADCP)	296 ± 5	332 ± 12	266 ± 31	323 ± 22
Phase (AOTIM-5)	**316**	**9**	**29**	**303**
Inclination (ADCP)	61 ± 5	69 ± 12	73 ± 30	80 ± 23
Inclination (AOTIM-5)	**57**	**60**	**60**	**64**
KH (74.7°N, 125.3°E)				
Major axis (ADCP)	5.6 ± 0.1	3.3 ± 0.1	1.0 ± 0.1	0.9 ± 0.07
Major axis (AOTIM-5)	**2.7**	**1.2**	**1.3**	**0.6**
Minor axis (ADCP)	−1.7 ± 0.1	−1.3 ± 0.1	−0.3 ± 0.1	−0.3 ± 0.1
Minor axis (AOTIM-5)	**−1.2**	**−0.3**	**−0.2**	**−0.1**
Phase (ADCP)	286 ± 1	333 ± 2	260 ± 7	340 ± 7
Phase (AOTIM-5)	**296**	**332**	**51**	**333**
Inclination (ADCP)	103 ± 1	101 ± 2	97 ± 8	84 ± 8
Inclination (AOTIM-5)	**93**	**109**	**80**	**79**
AN (74.3°N, 128.0°E)				
Major axis (ADCP)	5.4 ± 0.1	3.1 ± 0.2	1.1 ± 0.2	0.6 ± 0.1
Major axis (AOTIM-5)	**2.8**	**1.1**	**1.3**	**0.5**
Minor axis (ADCP)	0.4 ± 0.2	−0.2 ± 0.2	0.2 ± 0.1	−0.1 ± 0.2
Minor axis (AOTIM-5)	**−0.1**	**−0.2**	**0.2**	**0.1**
Phase (ADCP)	297 ± 2	354 ± 2	280 ± 6	351 ± 11
Phase (AOTIM-5)	**347**	**50**	**72**	**355**
Inclination (ADCP)	98 ± 2	103 ± 3	95 ± 8	104 ± 14
Inclination (AOTIM-5)	**80**	**92**	**69**	**66**
Y98 (75.2°N, 131°E)				
Major axis (ADCP)	6.3 ± 0.2	3.2 ± 0.2	1.1 ± 0.2	0.4 ± 0.2
Major axis (AOTIM-5)	**5.0**	**2.2**	**1.5**	**0.6**
Minor axis (ADCP)	−1.9 ± 0.1	−1.2 ± 0.1	−0.4 ± 0.1	−0.1 ± 0.1
Minor axis (AOTIM-5)	**−2.0**	**−1.0**	**−0.6**	**−0.3**
Phase (ADCP)	163 ± 2	112 ± 4	297 ± 15	138 ± 28
Phase (AOTIM-5)	**332**	**31**	**59**	**339**
Inclination (ADCP)	62 ± 1	62 ± 3	65 ± 8	62 ± 15
Inclination (AOTIM-5)	**64**	**68**	**63**	**63**

ellipse parameters, including major A_{maj} and minor A_{min} axes, inclination, and phase angles, and are compared with tidal characteristics from AOTIM-5 (Table 2). The tidal ellipse results from the combination of two counter-rotating circles (CW and CCW), which are computed according to

$$R(-) = \frac{A_{maj} - A_{min}}{2}(\text{CW}) \quad \text{and} \tag{1}$$

$$R(+) = \frac{A_{maj} + A_{min}}{2}(\text{CCW}). \tag{2}$$

For a first-order estimate of the barotropic tide at each mooring site, harmonic analysis was performed on year-long vertically averaged ADCP records. Note that the vertical averages exclude the upper ~10 m of the water column due to range limitations and/or disturbances caused by sea ice. In agreement with AOTIM-5, the four leading constituents of the moored observations are the principal lunar M_2 as the dominant constituent throughout the shelf, exceeding the second-strongest principal solar S_2 by a factor of 2, followed by the lunar elliptical N_2 and the semidiurnal lunisolar declinational constituent K_2. Most ellipse characteristics are in reasonably good agreement between observations and AOTIM-5, although in some locations the observed tidal magnitudes can significantly exceed the model values (Fig. 4; Table 2). Tidal ellipses are nearly circular on the outer shelf and increasingly eccentric near shore, where the currents are influenced by the shallow bathymetry. The rotation of all semidiurnal constituents is

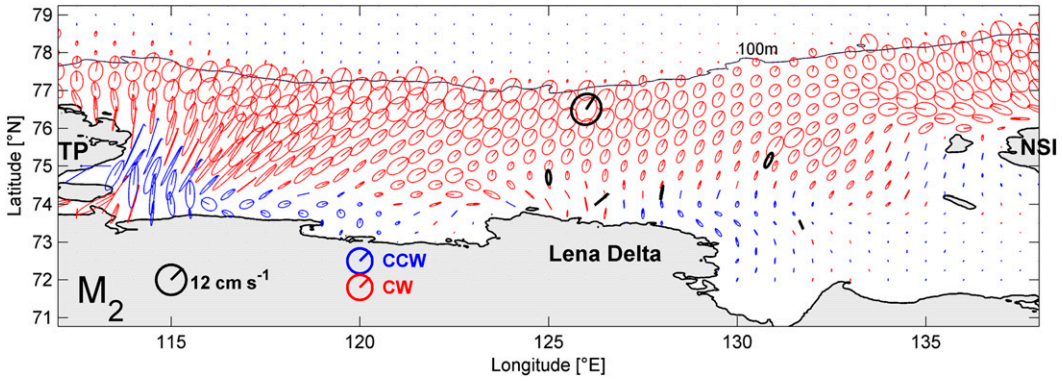

FIG. 4. M_2 tidal ellipses from AOTIM-5: red (CW) and blue (CCW) colors indicate the sense of rotation and inclination is given by the line inside the ellipses. Black ellipses indicate the ADCP-derived M_2 characteristics from the moorings. Scale of the tidal amplitude is given in the lower left, with major and minor axes of 12 cm s^{-1}. Note that for a clearer presentation, only one AOTIM-5 grid point is shown per degree longitude [2 (°lat)$^{-1}$]. Taymir Peninsula (TP) and New Siberian Islands (NSI) are marked for spatial reference (see also Fig. 1). Black contour outlines the 10-m isobath (IBCAO; Jakobsson et al. 2008). The Gulf of Khatanga mentioned in the text is located in the southwestern part of this figure, characterized by strong CCW tides.

predominantly clockwise except in the shallower nearshore regions, where tides are significantly weaker. The strongest tidal velocities are found on the outer shelf and, in particular, in the Gulf of Khatanga in the southwestern Laptev Sea, where resonance occurs (Kowalik and Proshutinsky 1994) and rotation switches to CCW (Fig. 4).

The year-round vertically averaged ADCP records across the Laptev Sea display strong fortnightly modulation due to the beating of M_2 with S_2 within a range of 5–20 cm s^{-1} between neap and spring cycles on the outer shelf (Fig. 5) and 3–10 cm s^{-1} on the inner shelf (Fig. 6), where the smaller tidal velocities are more irregular. In general, the OS record shows little seasonal variability, and tides explain ~71% of the outer shelf's variability based on a harmonic analysis over the entire record. Harmonic analyses, performed over 29-day overlapping segments necessary to resolve a synodic month, indicate that tides explain most of the variability (85%–95%) under a nearly 100% sea ice cover, while the importance of tides drops to 60%–80% in the open water season

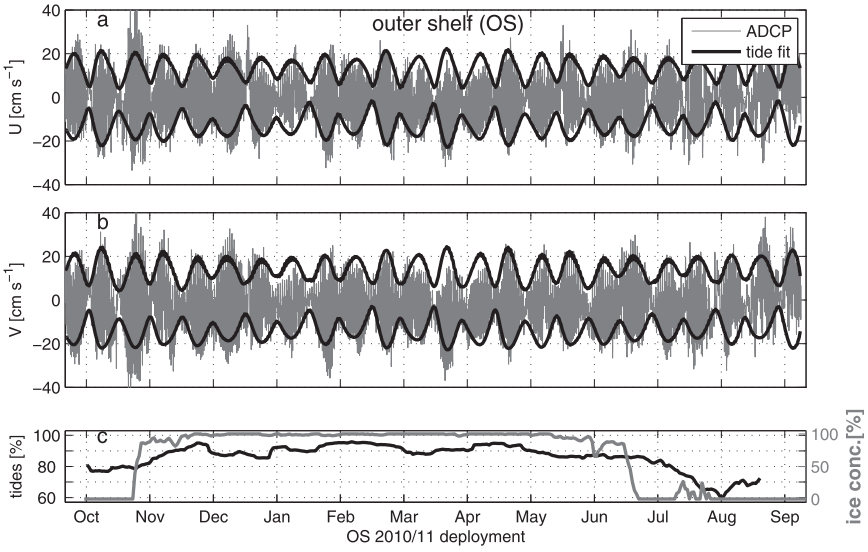

FIG. 5. 2010/11 time series of OS mooring depth–averaged (a) zonal and (b) meridional ADCP velocities (cm s^{-1}; gray) vs tidal fits (black) from harmonic analyses. Top (bottom) black lines show the max (min) tidal velocities within a semidiurnal tidal cycle, highlighting the fortnightly modulation of the tides. (c) Ratio of the tidal variability to the total variability of the ADCP data (black line) and SSM/I-based sea ice concentration (%; gray line).

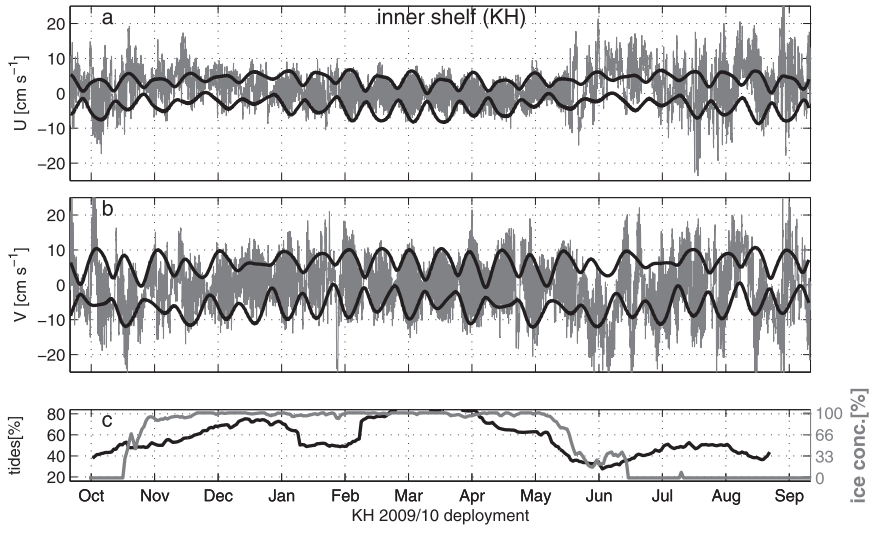

FIG. 6. As in Fig. 5, but for the 2009/10 KH deployment.

(Fig. 5c), when wind effects become more important. Tides similarly dominate the total current variability at KH when ice is present (Fig. 6). However, the portion of the variance accounted for by tides is lower in early winter compared with late winter despite nearly 100% ice concentration throughout. This is likely related to a thinner and more mobile early-winter ice cover (Janout et al. 2013), which may transfer stress at the ice–ocean interface more effectively than during late-winter/spring conditions, when ice is thick and landfast ice is present in shore of the mooring location. Although sea ice may dampen wind-generated inertial oscillations (Rainville and Woodgate 2009), they were shown to penetrate loose pack ice (Padman and Kottmeier 2000; Kwok et al. 2003) and can hence not be ignored even under a solid ice cover. For example, in January 2010 the current's variance explained by tides decreased to ~50%, coincident with increased meridional velocities (Fig. 6). This period was characterized by strong winds (>15 m s^{-1}) and large ice drift velocities in the bottom-track record, but without apparent reductions in the ice concentration (not shown).

In contrast to the total tidal current, individual tidal constituents show a considerable seasonal variability in both M_2 and S_2 tides (Figs. 7a,b). The depth-averaged M_2 CW tide is at a minimum during fall and nearly constant from December through July. However, S_2 shows a strong semiannual oscillation with minima of ~4 cm s^{-1} occurring in both December and June, and maxima in October (~9 cm s^{-1}) and March (~7 cm s^{-1}). The semiannual oscillation results from the superposition of the S_2 with the K_2 constituent (period of 182.6 days), with maximum velocities when the sun passes the equator during the equinoxes. The N_2 (not shown) is the weakest constituent without apparent seasonal signals. The inshore locations behave similarly at reduced magnitude.

c. Vertical structure of semidiurnal tides

Studying tides in the context of diapycnal mixing requires a detailed investigation into the vertical structure of the tides, as tidal baroclinicity is a source of shear. We subsampled our time series for the ice-covered periods, which we based on SSM/I sea ice concentration from

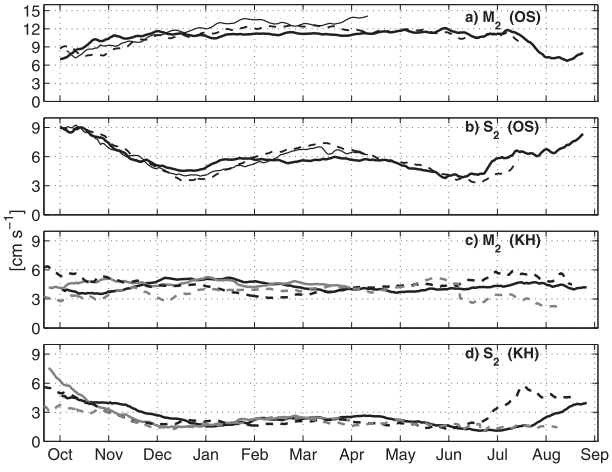

FIG. 7. Seasonal variability of depth-averaged CW currents of M_2 and S_2 from (a),(b) three OS and (c),(d) four KH deployments, computed from 29-day overlapping analyses. Lines correspond to the following years: OS (thick solid: 2010/11, dashed: 2006/07, thin solid: 2005/06); KH (solid black: 2007/08, solid gray: 2008/09, dashed black: 2009/10, dashed gray: 2010/11). Note that the semiannual peaks in S_2 result from the superposition with K_2.

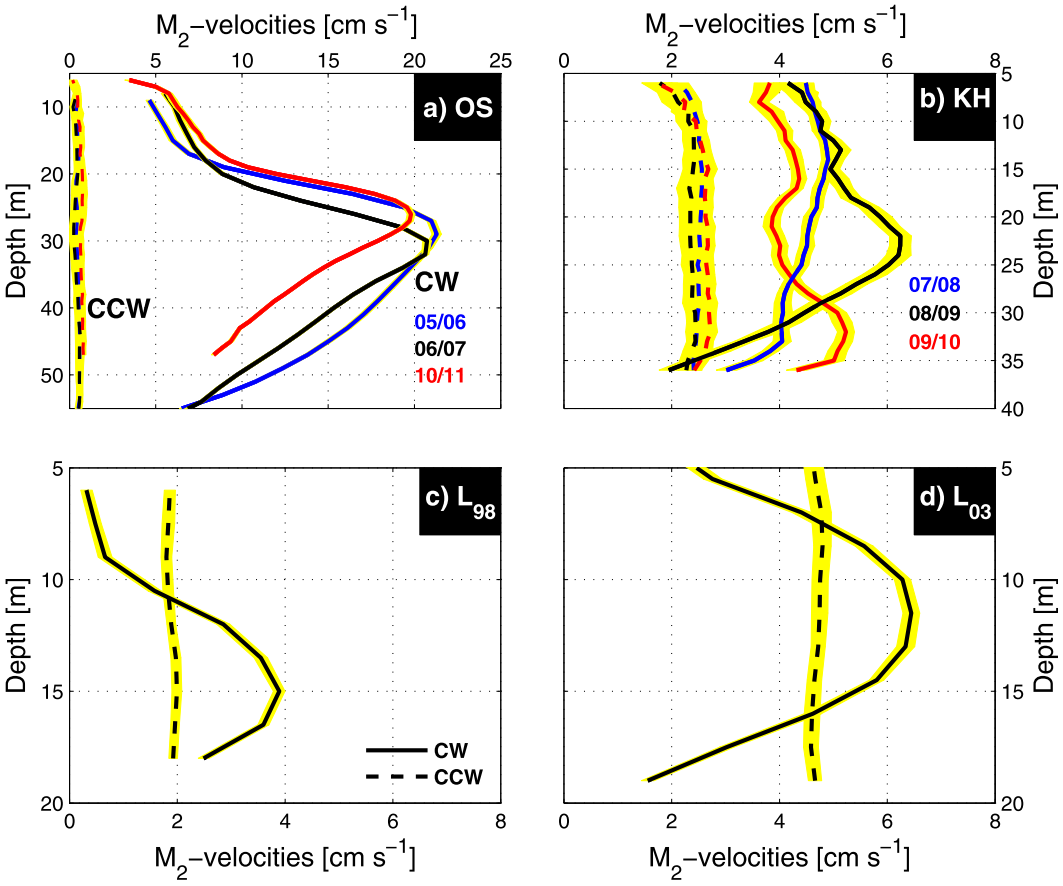

FIG. 8. Vertical structure of semidiurnal tides (cm s^{-1}) vs depth (m) at different locations computed from harmonic tidal analyses through the ice-covered seasons. Yellow shading shows 95% confidence limits. Note that the axis limits are not uniform in the four panels. Solid (dashed) lines indicate CW (CCW) currents in all panels: (a) OS: M_2 CW and CCW for all three deployments, (b) KH: M_2 CW and CCW for three deployments, (c) L98, and (d) L03.

the nearest grid point, in order to reduce the effect of wind-induced inertial motion in the ADCP data, and performed harmonic analysis on the individual depth levels (Fig. 8). Prandle (1982) and Foldvik et al. (1990) showed that, as the tidal frequency ω approaches the inertial frequency f, the Ekman boundary layers (BL) are separated in two independent layers, which scale according to

$$h^{-} = \left(\frac{A}{\omega - f}\right)^{0.5} \text{(CW)} \tag{3}$$

and

$$h^{+} = \left(\frac{A}{\omega + f}\right)^{0.5} \text{(CCW)}. \tag{4}$$

This implies that, with a constant eddy viscosity A, the CCW BL is constrained, while the CW BL may theoretically grow infinitely at the critical latitude, although it may be in reality bounded by stratification, as also pointed out by Kulikov et al. (2004). These considerations imply that vertical structures develop differently near the critical latitude, with a depth-dependent CW component and a nearly depth-uniform CCW component (Foldvik et al. 1990; Furevik and Foldvik 1996; Kulikov et al. 2004), which then has implications for shear and vertical mixing.

As expected, each mooring record shows a dominance of the CW component over the CCW component. CCW components are depth uniform without exceptions, while CW components in most locations (except AN) are highly depth dependent (Figs. 8, 9). The three OS deployments consistently display pronounced midwater maxima in their CW components in both M_2 and S_2 (not shown) constituents (Fig. 8a), located near the depth of the seasonal pycnocline in September (Fig. 10, described in greater detail below). Midwater maxima in M_2 CW currents are apparent even in those moorings located

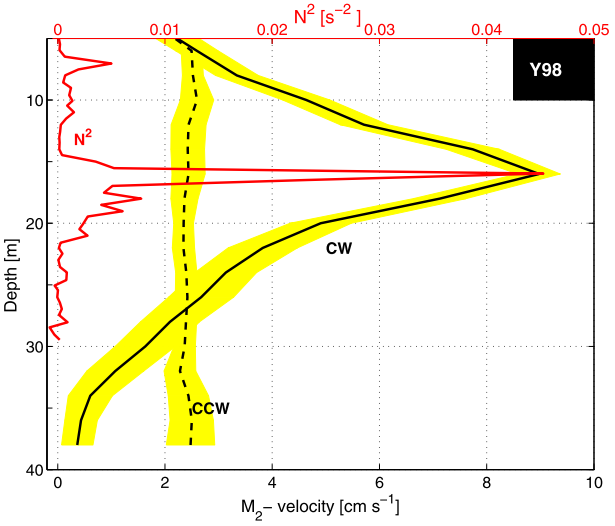

FIG. 9. CW and CCW M_2 currents from the mooring Y98, and stratification derived from a CTD profile from 6 May 1999 near the mooring location. Tidal currents presented here were derived from harmonic analysis over a 30-day period surrounding 6 May 1999.

under landfast ice (L98 and L03), where stratification can prevail throughout the winter despite the shallow bathymetry. Two out of three KH deployments feature comparatively depth-uniform M_2 CW currents, although those may present a somewhat misleading picture related to the varying vertical structure through the course of a winter as shown by Janout et al. (2013) and as will be discussed later.

The relationship between stratification and the vertical tidal structure was previously shown in numerous studies (e.g., Visser et al. 1994; Souza and Simpson 1996; Makinson et al. 2006; Danielson and Kowalik 2005), and is additionally reemphasized by inspecting the few available under-ice CTD profiles that were taken at or in the vicinity of the mooring locations during an ADCP recording period. In particular, Y98 features sharp peaks in tides and stratification (Fig. 9), overall highlighting the impact of stratification on the baroclinicity of tidal currents, which has important consequences for diapycnal mixing processes on this shelf.

d. Interannual comparison of semidiurnal tides and shear

Stratification is crucial for understanding tidal dynamics, yet it is difficult to quantify with moorings in shallow ice-covered seas. However, the limited information that is available from the Laptev Sea shelf shows a positive relationship between shear and stratification (not shown), confirming that shear is generally strongest in the pycnocline (van Haren 2000; Howard et al. 2004). This relationship allows us to use the maximum shear level as an indicator for mixed layer depth and hence to qualitatively understand the connections between stratification, shear, tides, and sea ice.

The variability of the tidal currents displays links to sea ice concentration, near-bottom temperature, and salinity (Fig. 11: KH; Fig. 12: OS; both described in greater detail below) and indicates some contrasting dynamics between the inner and outer shelves. Basic differences of the two sites KH and OS are water depth (43 and ~60 m, respectively) and the proximity to the Lena freshwater source. The M_2 currents at KH include inertial currents due to similar frequencies, and hence each summer and fall KH shows enhanced wind-driven currents near the surface. After the freeze-up, surface currents decrease and downward-progressing internal shear maxima are observed in each of the 4 years, reflecting a downward-progressing pycnocline. Interannual differences in the vertical structure of tides and shear hence result from differences in water column structures. Although winter stratification on the inner shelf is to a large degree governed by the (wind driven) distribution of the Lena freshwater plume during the previous summer (Dmitrenko et al. 2010), diapycnal mixing also features in the Laptev Sea's mixed layer dynamics. The deepening of the pycnocline in winter is likely a result of a series of destabilizing forces such as tide-/shear-induced mixing, surface stress from ice motion, storm, and polynya events, or buoyancy loss during ice formation. In years with "average" stratification (Fig. 10), the mixing may be strong enough to erode stratification completely and lead to barotropic tidal structures by spring (e.g., spring of 2008 and 2011 in Fig. 11), but not in years with anomalously strong stratification (2008–09). The internal tidal maximum that appears in February 2010 despite the weak initial stratification, however, is a consequence of stratification induced by a near-bottom inflow of dense water from the shelf break (Janout et al. 2013). This 4-yr-long record shows a wide range of near-bottom temperature and salinity (from $-1.8°$ to $>0°$C and 29.5–33.5) and implies that the inner shelf can be shaped by three-dimensional processes, complicating the prediction of vertical tidal structure and shear.

OS is farther away from the Lena outflow and hence the salinity is higher than at KH (Fig. 10) and its variability there is to first order dominated by the seasonal freeze and melt cycle. One major difference to KH is the persistence of the OS pycnocline near 20 m. Similar to KH, M_2 tides are at a maximum below the pycnocline once an ice cover has developed, and weaken through the course of a winter until baroclinic tidal structures nearly recede by mid- to late spring (in 2 out of 3 years) (Fig. 12). In both of those years (April 2007 and March 2011), the recession of the shear at the pycnocline

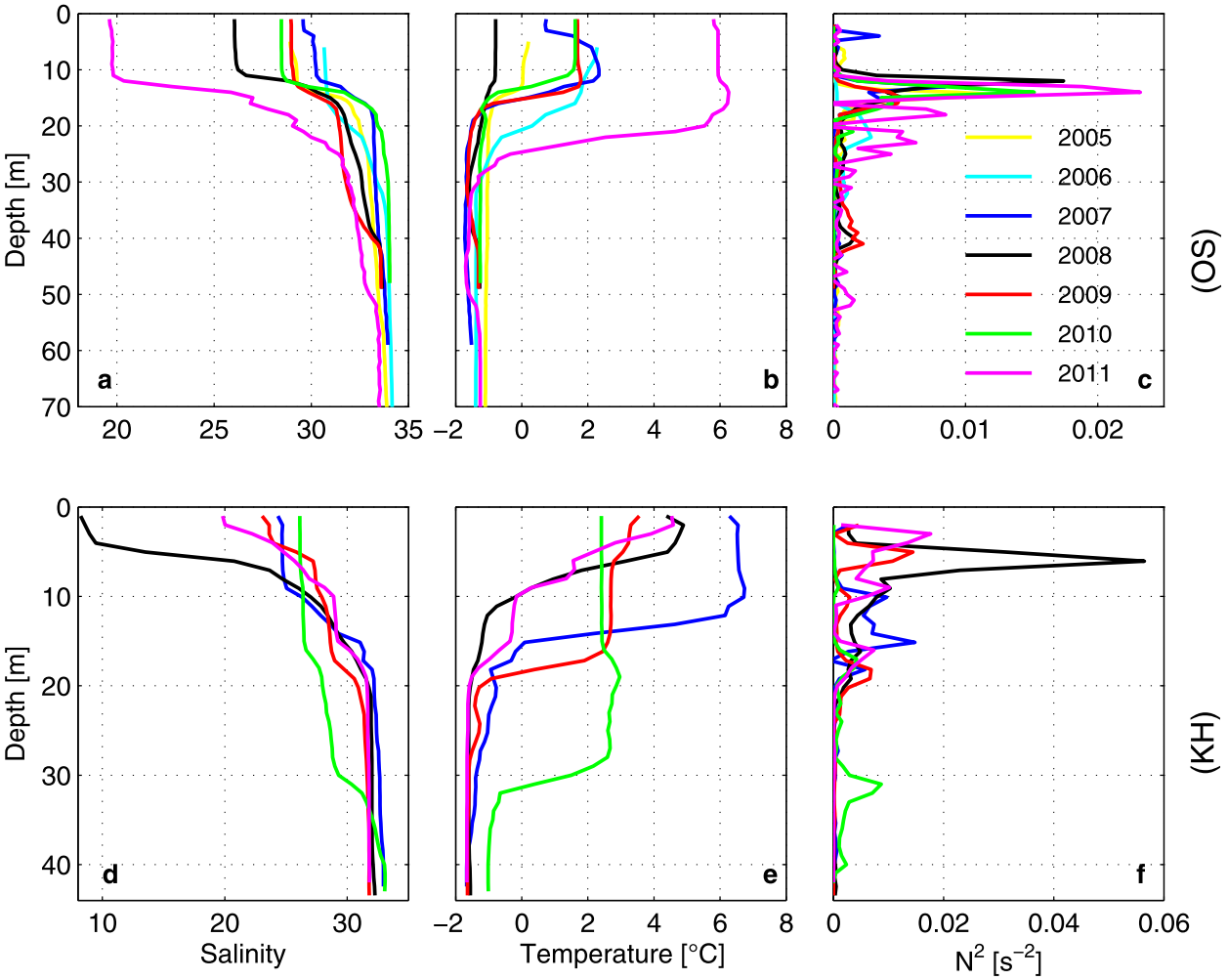

FIG. 10. Summer CTD profiles from the (a),(c) OS (2005–11) and (d),(f) KH (2007–11) for salinity (left) temperature (°C) (middle), and N^2 (s^{-2}) (right), indicating interannual variations in late-summer water column structures. Color code in (c) applies to all panels. Note that the axis limits are not uniform.

coincides with enhanced ice drift (not shown) and changes in the bottom water properties. While a more precise description of the development of the hydrographic structure on this shelf requires additional observations, our time series suggest that the processes acting on the inner shelf may be more complex than on the outer shelf. The tidal dynamics in both regions, however, appear to be closely influenced by the presence of sea ice.

e. *On the relative importance of tides under ice versus open water*

Because the dominant issues on Arctic shelves evolve around the changing sea ice conditions, we revisited our mooring records to obtain a better understanding of the relative importance of tides under sea ice versus open water current regimes across the shelf. For that purpose and with help from SSM/I sea ice concentration records, we ran tidal analyses on three subsets of each of the 12 ADCP records, which were divided into three periods: 1) the pre-ice season: from the beginning of the mooring deployment (late August/early September) until a sea ice concentration of 90% is reached, 2) the ice season: sea ice concentrations >90%, and 3) the post-ice season: from when sea ice recedes to <90% until the end of the deployment. Then, we compared the variance of tides for each period with the total variance in depth-averaged currents (Fig. 13). We again note that this analysis excludes the uppermost ~10 m of the water column due to range limitations of ADCPs and/or errors associated with rough under-ice topography, and hence the total variance—in particular, during the open water seasons—is underestimated. Nevertheless, these limitations apply equally to all

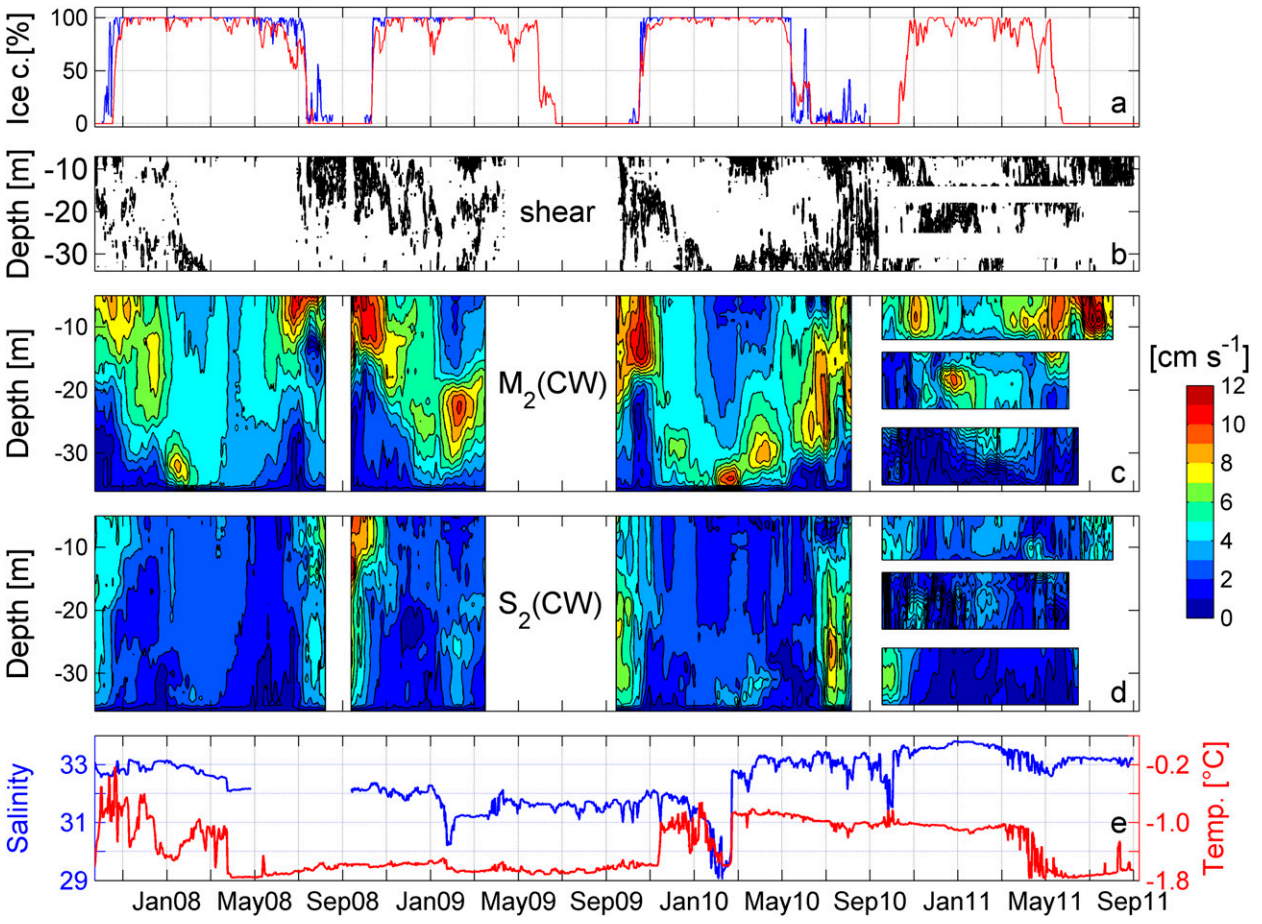

FIG. 11. Sea ice and ocean properties at KH from four mooring deployments between September 2007 and September 2011. (a) SSM/I-based (red) and bottom-track-derived (blue) sea ice concentration (%). (b) Semidiurnal shear $>0.02\,s^{-1}$ from bandpass-filtered ADCP data. CW component of the (c) M_2 and (d) S_2 tide is derived from KH ADCP data with 29-day overlapping harmonic analysis. Note that the inertial frequency is similar to the M_2 frequency at this location. (e) Near-bottom salinity (blue) and temperature (°C; red). Color bar applies to (c) and (d). Note that the white spaces in 2010/11 in (c) and (d) are data gaps between the three different 1200-kHz ADCPs used in that deployment (see also Table 1).

mooring records and justify this comparison, which overall suggests contrasting conditions between the current regimes on the outer and inner shelves. All three OS records display a variance that is on average higher than the other moorings, largely unaffected by sea ice, and mostly (>80%) explained by tides (Fig. 13b). In contrast to OS, all other locations show considerably lower variance under ice cover with on average 50% explained by tides. However, at these inner shelf stations, the total variance increases sharply with open water (Fig. 13a), and the relative importance of tides decreases (Fig. 13b). Interannual differences in the variance—for instance, at KH—reflect the increasing effect of winds on these shallower locations.

These results imply that reductions in the sea ice cover will overall increase the variance of Laptev Sea currents and decrease the predictability due to a decreasing importance of tides. Overall, it can be expected that shorter ice seasons will increase the wind energy input and increase the vertical dispersion of freshwater near the Lena outflow, which may potentially decrease stratification unless this effect is offset by an increase in river discharge to the Arctic shelves (Peterson et al. 2002). Except for the deeper outer shelf regions, these consequences may be expected for most of the Laptev Sea, considering that ~80% (~90%) of the shelf south of 76.5°N and west of 140°E is shallower than 40 m (50 m) (International Bathymetric Chart of the Arctic Ocean; Jakobsson et al. 2008).

5. Discussion and conclusions

Microstructure transects across the Laptev Sea shelf revealed episodes of intense dissipation rates of turbulent

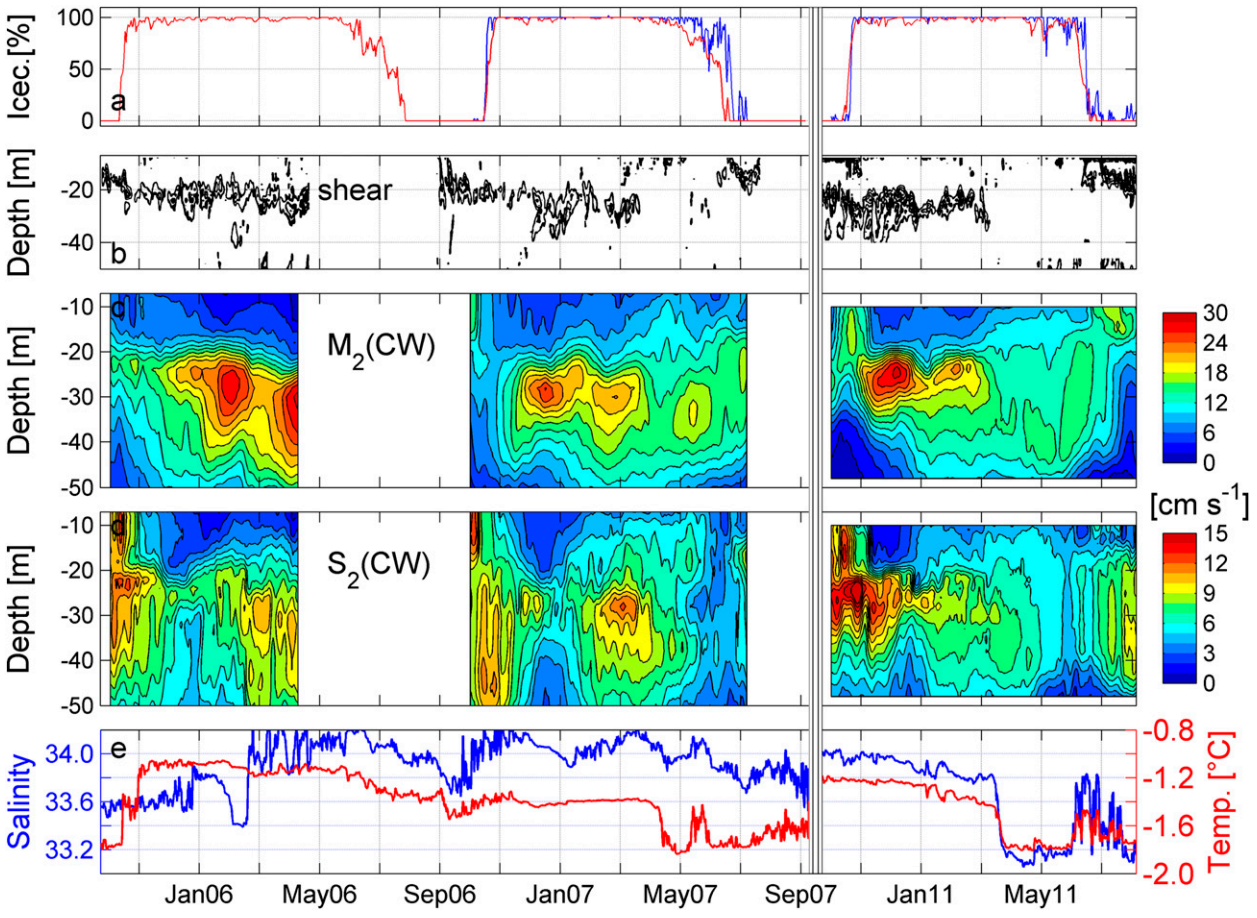

FIG. 12. As in Fig. 11, but for three OS deployments from 2005 to 2007 and from 2010 to 2011. The 2005/06 deployment provided no bottom-track data.

kinetic energy. Because most of the kinetic energy is in the semidiurnal frequency band, the motivation for this paper was to better understand semidiurnal tides, including their vertical structure and temporal and spatial variability, and their importance for diapycnal mixing. Harmonic analysis on 12-year-round ADCP records from six different locations across the Laptev Sea shelf (Fig. 1) showed that (i) barotropic tides vary spatially (in agreement with AOTIM-5; Fig. 4); (ii) the currents on the outer shelf are dominated by tides year-round, while on the shallower (<40 m) inner shelf, particularly under landfast ice, tides are less important when sea ice is absent (Fig. 13); and (iii) baroclinic tidal structures are strongly coupled to stratification throughout the shelf (Figs. 8, 9, 11, 12).

The close links between stratification, tides, and shear likely have consequences for the Laptev Sea's mixing environment. L11 invoked a mechanism proposed by BR09 to explain a striking episode of intense pycnocline dissipation observed during a 12-h time series of microstructure measurements taken under 100% ice cover in the northeast Laptev Sea near the continental shelf break. BR09 predict that intermittent peaks in shear that may drive turbulent mixing depend on the relative alignment between a rotating shear vector and the surface stress. In L11, the northeastern Laptev Sea currents were assumed to be dominated by a baroclinic tide and subject to surface forcing from the drifting ice. Here, we extended L11's assessment of the BR09 mechanism for open water conditions across a wider swath of the Laptev Sea, using the September 2007 microstructure transects (Fig. 2) taken under relatively steady wind conditions, in spatial and temporal proximity to our long-term moorings (KH and OS, Fig. 1). Our results indicate that BR09 finds year-round application across the Laptev Sea shelf, emphasizing the role of tides for predicting the occurrence of shear spike production and diapycnal mixing in a sheared water column. For example, tidal currents inferred from the KH and OS moorings and predicted by AOTIM-5 for

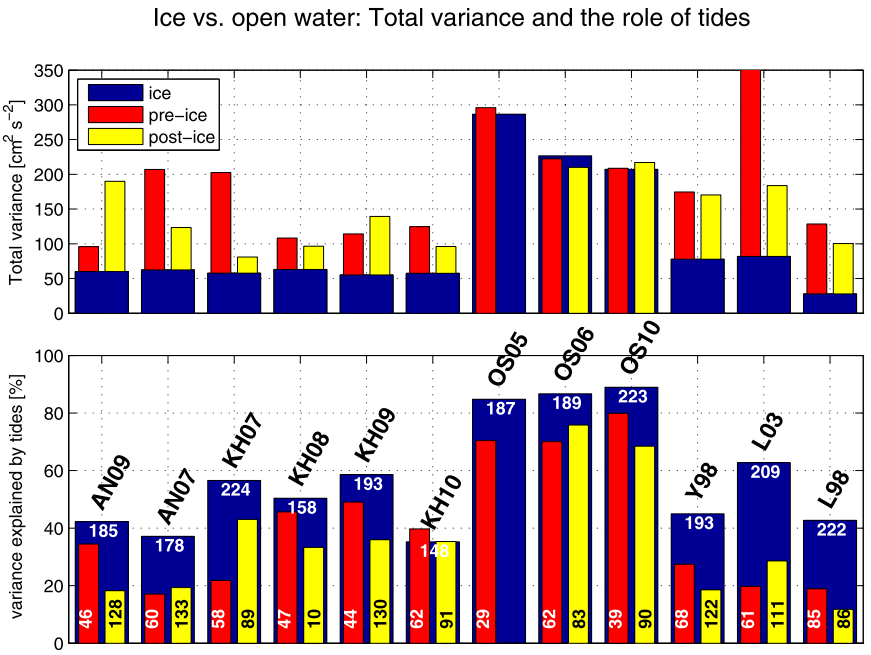

FIG. 13. (a): Total variance (cm^2 s^{-2}) in depth-averaged ADCP currents during the ice season (ice season, where sea ice concentration is >90%, blue), as well as pre- (red) and post-ice (yellow) season for all 12 mooring deployments. (b) Ratio of the tidal to the total variance (%) for these three time periods. Mooring name and year of all 12 deployments are written in black text. Numbers on bars indicate the duration (days) of each season, i.e., the number of days used for the harmonic analysis.

the 126°E section (Fig. 14b) imply a semidiurnally rotating current shear at the pycnocline (Fig. 14c) which, as predicted by BR09, is aligned with 6-hourly National Centers for Environmental Prediction (NCEP) winds (Kalnay et al. 1996; Kistler et al. 1999) immediately preceding the observed high pycnocline dissipation (Fig. 14a).

Wind forcing will also drive inertial (here, very close to semidiurnal) shear across the pycnocline and result in higher shear-driven dissipation than the tides alone can account for. Nonetheless, given their predictability, the tides may remain useful in predicting the phasing of shear spiking. Furthermore, considering that winds move an open water surface faster than a pack ice cover, ever higher diapycnal mixing rates can be expected under future scenarios of reduced sea ice. Our observations as well as high-resolution three-dimensional modeling studies of tides in the Arctic (Chen et al. 2009) stress the importance of stratification on tidal structures and vertical shear, and future changes in the mixing environment will at least partly depend on changes in stratification. Those, however, are far from being understood, and depend on a variety of factors including changes in winds and sea ice timing, as well as on timing, volume, and distribution of river runoff.

The recent years featured several minimum sea ice records that are linked to large-scale atmospheric pressure patterns such as the Arctic dipole anomaly (Wu et al. 2006), and generally imply increasing meridional winds over the Siberian shelves in summer (Overland et al. 2012), with several consequences for the Laptev Sea. First, an early off-shelf sea ice export likely extends the open water season, which may lead to fundamental shifts in the Laptev Sea's environment. Specifically, the Lena River freshwater plume encounters more energetic tides (and tidal mixing) when advected to the northern and northeastern Laptev Sea slope (Fig. 4). Consequently, stratification increases there, but it also enhances the tide-induced diapycnal mixing of coastal freshwater at the shelf break, which then may have consequences for the freshwater budget of the Arctic halocline (Aagaard et al. 1981).

Overall, tides dominate the shelf's dynamics but depend on season, stratification, and location, with an inner shelf that is more difficult to predict, due to the comparatively smaller role of tides there than on the deeper outer shelf. Hence, these results clearly emphasize the three-dimensionality of this shelf and imply that future modeling efforts designed to predict the physical and biogeochemical environment under a changing

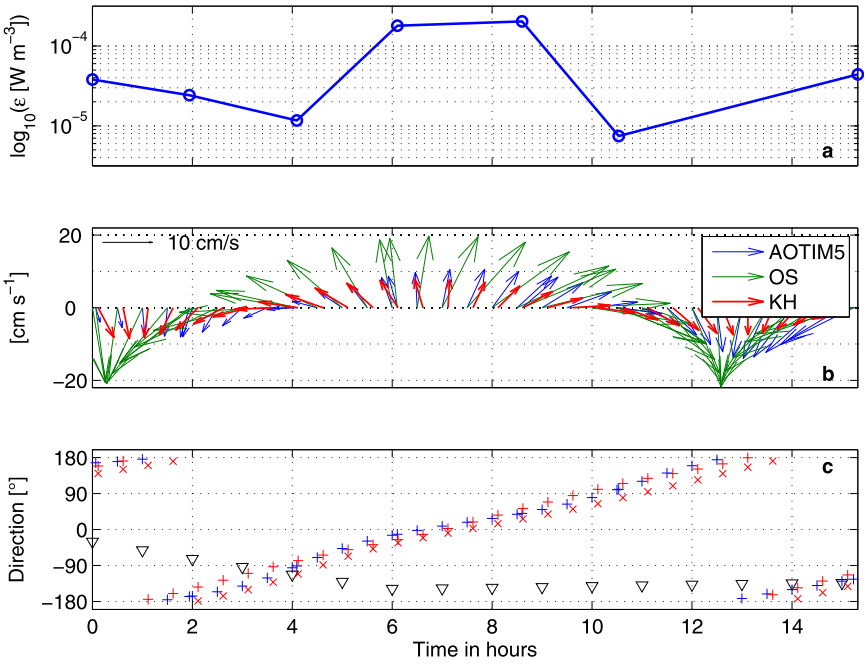

FIG. 14. (a) Max ε (W m^{-3}) within the 10–17-m pycnocline layer for each station along the 126°E transect. (b) AOTIM-5 tidal speeds (cm s^{-1}; blue), depth-averaged tidal fit to KH ADCP currents (red), and OS ADCP currents (green). (c) Direction (°) of NCEP wind stress (black triangles), AOTIM-5 tides (blue crosses), and KH least squares tides (red crosses). Time (h) is shown at the bottom of (c).

climate must accurately resolve the complex interplay among freshwater, tides, winds, sea ice, and landfast ice.

Acknowledgments. Financial support for the Laptev Sea System project was provided by the German Federal Ministry of Education and Research (Grant BMBF 03G0759B and 03G0833B) and the Ministry of Education and Science of the Russian Federation. The microstructure data were collected under the U.K. Natural Environment Research Council ASBO Arctic IPY Consortium Grant, with additional support for the analysis provided by a NERC Postdoctoral Fellowship. We greatly acknowledge Heidi Kassens and Leo Timokhov for managing the Laptev Sea projects. We thank the captains and crews of the various research vessels involved in the data collection. Much of the mooring data collection is owed to the efforts of Jens Hölemann. We sincerely thank the editor, Laurie Padman, and Luc Rainville for their constructive reviews, which greatly improved the paper.

REFERENCES

Aagaard, K., L. K. Coachman, and E. C. Carmack, 1981: On the halocline of the Arctic Ocean. *Deep-Sea Res.,* **28,** 529–545.

Alexandrov, V. Y., T. Martin, J. Kolatschek, H. Eicken, M. Kreyscher, and A. P. Makshtas, 2000: Sea ice circulation in the Laptev Sea and ice export to the Arctic Ocean: Results from satellite remote sensing and numerical modeling. *J. Geophys. Res.,* **105** (C7), 17 143–17 159.

Bareiss, J., and K. Görgen, 2005: Spatial and temporal variability of sea ice in the Laptev Sea: Analyses and review of satellite passive-microwave data and model results, 1979 to 2002. *Global Planet. Change,* **48,** 28–54.

Bauch, D., I. A. Dmitrenko, S. A. Kirillov, C. Wegner, J. Hölemann, S. Pivovarov, L. A. Timokhov, and H. Kassens, 2009: Eurasian Arctic shelf hydrography: Exchange and residence time of southern Laptev Sea waters. *Cont. Shelf Res.,* **29,** 1815–1820, doi:10.1016/j.csr.2009.06.009.

Burchard, H., and T. P. Rippeth, 2009: Generation of bulk shear spikes in shallow stratified tidal seas. *J. Phys. Oceanogr.,* **39,** 969–985.

Cavalieri, D., C. Parkinson, P. Gloersen, and H. J. Zwally, 2008: Sea ice concentrations from *Nimbus-7* SMMR and DMSP SSM/I-SSMIS passive microwave data, 1998-2011. National Snow and Ice Data Center, Boulder, CO, digital media.

Chen, C., G. Gao, J. Qi, A. Proshutinsky, R. C. Beardsley, Z. Kowalik, H. Lin, and G. Cowles, 2009: A new high-resolution unstructured grid finite volume Arctic Ocean model (AO-FVCOM): An application for tidal studies. *J. Geophys. Res.,* **114,** C08017, doi:10.1029/2008JC004941.

Danielson, S., and Z. Kowalik, 2005: Tidal currents in the St. Lawrence Island region. *J. Geophys. Res.,* **110,** C10004, doi:10.1029/2004JC002463.

D'Asaro, E. A., and J. H. Morison, 1992: Internal waves and mixing in the Arctic Ocean. *Deep-Sea Res.,* **39,** S459–S484.

Dmitrenko, I. A., and Coauthors, 2010: Wind-driven diversion of summer river runoff preconditions the Laptev Sea coastal polynya hydrography: Evidence from summer-to-winter hydrographic records of 2007–2009. *Cont. Shelf Res.,* **30,** 1656–1664, doi:10.1016/j.csr.2010.06.012.

——, S. A. Kirillov, E. Bloshkina, and Y.-D. Lenn, 2012: Tide-induced vertical mixing in the Laptev Sea coastal polynya. *J. Geophys. Res.,* **117,** C00G14, doi:10.1029/2011JC006966.

Fer, I., 2009: Weak vertical diffusion allows maintenance of cold halocline in the central Arctic. *Atmos. Oceanic Sci. Lett.,* **2,** 148–152.

——, R. Skogseth, and F. Geyer, 2010: Internal waves and mixing in the marginal ice zone near the Yermak Plateau. *J. Phys. Oceanogr.,* **40,** 1613–1630.

Foldvik, A., J. H. Middleton, and T. D. Foster, 1990: The tides of the southern Weddell Sea. *Deep-Sea Res.,* **37,** 1345–1362.

Furevik, T., and A. Foldvik, 1996: Stability at M_2 critical latitude in the Barents Sea. *J. Geophys. Res.,* **101** (C4), 8823–8837.

Gonella, J., 1972: A rotary-component method for analysing meteorological and oceanographic vector time series. *Deep-Sea Res.,* **19,** 833–846.

Guay, C. K. H., K. K. Falkner, R. D. Muench, M. Mensch, M. Frank, and R. Bayer, 2001: Wind-driven transport pathways for Eurasian Arctic river discharge. *J. Geophys. Res.,* **106** (C6), 11 469–11 480.

Hölemann, J. A., S. Kirillov, T. Klagge, A. Novikhin, H. Kassens, and L. Timokhov, 2011: Near-bottom water warming in the Laptev Sea in response to atmospheric and sea-ice conditions in 2007. *Polar Res.,* **30,** 6425, doi:10.3402/polar.v30i0.6425.

Holland, M. M., J. Finnis, and M. C. Serreze, 2006: Simulated Arctic Ocean freshwater budgets in the twentieth and twenty-first centuries. *J. Climate,* **19,** 6221–6242.

Howard, S. L., J. Hyatt, and L. Padman, 2004: Mixing in the pycnocline over the western Antarctic Peninsula shelf during Southern Ocean GLOBEC. *Deep-Sea Res. II,* **51,** 1965–1979, doi:10.1016/j.dsr2.2004.08.002.

Jakobsson, M., R. Macnab, L. Mayer, R. Anderson, M. Edwards, J. Hatzky, H. W. Schenke, and P. Johnson, 2008: An improved bathymetric portrayal of the Arctic Ocean: Implications for ocean modeling and geological, geophysical and oceanographic analyses. *Geophys. Res. Lett.,* **35,** L07602, doi:10.1029/2008gl033520.

Janout, M. A., J. Hölemann, and T. Krumpen, 2013: Cross-shelf transport of warm and saline water in response to sea ice drift on the Laptev Sea shelf. *J. Geophys. Res.,* **118,** 563–576, doi:10.1029/2011JC007731.

Kalnay, E., and Coauthors, 1996: The NCEP/NCAR 40-Year Reanalysis Project. *Bull. Amer. Meteor. Soc.,* **77,** 437–471.

Kistler, R., and Coauthors, 1999: The NCEP–NCAR 50-Year Reanalysis: Monthly means CD-ROM and documentation. *Bull. Amer. Meteor. Soc.,* **82,** 247–267.

Kowalik, Z., and A. Yu. Proshutinsky, 1993: Diurnal tides in the Arctic Ocean. *J. Geophys. Res.,* **98** (C9), 16 449–16 468.

——, and ——, 1994: The Arctic Ocean tides. *The Polar Oceans and Their Role in Shaping the Global Environment, Geophys. Monogr.,* Vol. 85, Amer. Geophys. Union, 137–158, doi:10.1029/GM085p0137.

Krumpen T., M. Janout, K. I . Hodges, R. Gerdes, F. Girard-Ardhuin, J. A. Hölemann, and S. Willmes, 2013: Variability and trends in Laptev Sea ice outflow between 1992–2011. *Cryosphere,* **7,** 349–363.

Kulikov, E. A., A. B. Rabinovich, and E. C. Carmack, 2004: Barotropic and baroclinic tidal currents on the Mackenzie shelf break in the southeastern Beaufort Sea. *J. Geophys. Res.,* **109,** C05020, doi:10.1029/2003JC001986.

Kwok, R., G. F. Cunningham, and W. D. Hibler III, 2003: Sub-daily ice motion and deformation from RADARSAT observations. *Geophys. Res. Lett.,* **30,** 2218, doi:10.1029/2003GL018723.

Lenn, Y.-D., and Coauthors, 2009: Vertical mixing at intermediate depths in the Arctic boundary current. *Geophys. Res. Lett.,* **36,** L05061, doi:10.1029/2008GL036792.

——, T. P. Rippeth, C. P. Old, S. Bacon, I. Polyakov, V. Ivanov, and J. Hölemann, 2011: Intermittent intense turbulent mixing under ice in the Laptev Sea continental shelf. *J. Phys. Oceanogr.,* **41,** 531–547.

Makinson, K., M. Schröder, and S. Østerhus, 2006: Effect of critical latitude and seasonal stratification on tidal current profiles along Ronne Ice Front, Antarctica. *J. Geophys. Res.,* **111,** C03022, doi:10.1029/2005JC003062.

Nøst, E., 1994: Calculating tidal current profiles from vertically integrated models near the critical latitude in the Barents Sea. *J. Geophys. Res.,* **99** (C4), 7885–7901.

Overland, J. E., J. A. Francis, E. Hanna, and M. Wang, 2012: The recent shift in early summer Arctic atmospheric circulation. *Geophys. Res. Lett.,* **39,** L19804, doi:10.1029/2012GL053268.

Padman, L., and T. M. Dillon, 1991: Turbulent mixing near the Yermak Plateau during the Coordinated Eastern Arctic Experiment. *J. Geophys. Res.,* **96** (C3), 4769–4782.

——, and C. Kottmeier, 2000: High-frequency ice motion and divergence in the Weddell Sea. *J. Geophys. Res.,* **105** (C2), 3379–3400.

——, and S. Erofeeva, 2004: A barotropic inverse tidal model for the Arctic Ocean. *Geophys. Res. Lett.,* **31,** L02303, doi:10.1029/2003GL019003.

Pawlowicz, R., B. Beardsley, and S. Lentz, 2002: Classical tidal harmonic analysis including error estimates in MATLAB using T_TIDE. *Comput. Geosci.,* **28,** 929–937.

Peterson, B. J., R. M. Holmes, J. W. McClelland, C. J. Vörösmarty, R. B. Lammers, A. I. Shiklomanov, I. A. Shiklomanov, and S. Rahmstorf, 2002: Increasing river discharge to the Arctic Ocean. *Science,* **298,** 2171–2173.

Polyakov, I. V., A. Pnyushkov, R. Rember, V. V. Ivanov, Y.-D. Lenn, L. Padman, and E. C. Carmack, 2012: Mooring-based observations of the double-diffusive staircases over the Laptev Sea slope. *J. Phys. Oceanogr.,* **42,** 95–109.

Prandle, D., 1982: The vertical structure of tidal currents and other oscillatory flows. *Cont. Shelf Res.,* **1,** 191–207.

Rainville, L., and P. Winsor, 2008: Mixing across the Arctic Ocean: Microstructure observations during the Beringia 2005 expedition. *Geophys. Res. Lett.,* **35,** L08606, doi:10.1029/2008GL033532.

——, and R. A. Woodgate, 2009: Observations of internal wave generation in the seasonally ice-free Arctic. *Geophys. Res. Lett.,* **36,** L23604, doi:10.1029/2009GL041291.

Robertson, R., 2001: Internal tides and baroclinicity in the southern Weddell Sea: 2. Effects of the critical latitude and stratification. *J. Geophys. Res.,* **106** (C11), 27 017–27 034.

Rudels, B., G. Björk, R. Muench, and U. Schauer, 1999: Double-diffusive layering in the Eurasian Basin of the Arctic Ocean. *J. Mar. Syst.,* **21,** 3–27.

Shpaikher, O., Z. P. Fedorova, and Z. S. Yankina, 1972: Interannual variability of hydrological regime of the Siberian shelf seas in response to atmospheric processes (in Russian). *Proc. Arct. Antarct. Res. Inst.,* **306,** 5–17.

Souza, A. J., and J. H. Simpson, 1996: Interaction between mean water column stability and tidal shear in the production of

semi-diurnal switching of stratification in the Rhine ROFI. *Buoyancy Effects on Coastal and Estuarine Dynamics,* D. G. Aubrey and C. T. Friedrichs, Eds., Coastal Estuarine Studies, Vol. 53, Amer. Geophys. Union, 83–96.

Stedmon, C. A., R. M. W. Amon, A. J. Rinehart, and S. A. Walker, 2011: The supply and characteristics of colored dissolved organic matter (CDOM) in the Arctic Ocean: Pan Arctic trends and differences. *Mar. Chem.,* **124,** 108–118.

Stroeve, J., M. C. Serreze, S. Drobot, S. Gearhead, M. M. Holland, J. Maslanik, W. Meier, and T. Scambos, 2008: Arctic sea ice plummets in 2007. *Eos, Trans. Amer. Geophys. Union,* **89,** 13–14, doi:10.1029/2008EO020001.

Sundfjord, A., I. Fer, Y. Kasajima, and H. Svendsen, 2007: Observations of turbulent mixing and hydrography in the marginal ice zone of the Barents Sea. *J. Geophys. Res.,* **112,** C05008, doi:10.1029/2006JC003524.

Timmermans, M.-L., J. Toole, R. Krishfield, and P. Winsor, 2008: Ice-tethered profiler observations of the double-diffusive staircase in the Canada Basin thermocline. *J. Geophys. Res.,* **113,** C00A02, doi:10.1029/2008JC004829.

van Haren, H., 2000: Properties of vertical current shear across stratification in the North Sea. *J. Mar. Res.,* **58,** 465–491.

Visser, A. W., A. J. Souza, K. Hessner, and J. H. Simpson, 1994: The effect of stratification on tidal current profiles in the region of freshwater influence. *Oceanol. Acta,* **17,** 369–381.

Vlasenko, V., N. Stashchuk, K. Hutter, and K. Sabinin, 2003: Nonlinear internal waves of tidal periods at critical latitudes. *Deep-Sea Res. I,* **50,** 317–338.

Wegner, C., and Coauthors, 2013: Interannual variability of surface and bottom sediment transport on the Laptev Sea shelf during summer. *Biogeosciences,* **10,** 1117–1129, doi:10.5194/bg-10-1117-2013.

Wu, B., J. Wang, and J. E. Walsh, 2006: Dipole anomaly in the winter Arctic atmosphere and its association with sea ice motion. *J. Climate,* **19,** 210–225.

Zakharov, V. F., 1966: The role of flaw leads off the edge of fast ice in the hydrological and ice regime of the Laptev Sea. *Oceanology,* **6,** 815–821.